Feedforward Control of Deformable Membrane Mirrors for Adaptive Optics

Thomas Ruppel, Shihao Dong, Frédéric Rooms, Wolfgang Osten, and Oliver Sawodny

***Abstract*—In this paper, performance enhancements for deformable membrane mirrors based on model-based feedforward control are presented. The investigated deformable mirror consists of a flexible membrane and voice coil actuators. Feedback control of the distributed actuators cannot be implemented in these mirrors due to a lack of high speed internal position measurements of the membrane's deformation. However, by using feedforward control, the dominant dynamics of the membrane can still be controlled allowing for faster settling times and reduced membrane vibrations. Experimental results are presented for an ALPAO deformable mirror with 88 distributed actuators on a circular membrane with a pupil of two centimeters in diameter.**

***Index Terms*—Adaptive optics, deformable membrane mirror, distributed parameter system, feedforward control.**

I. Introduction

THE USE of deformable mirrors (DMs) in adaptive optics (AO) systems allows for the compensation of various external and internal optical disturbances. For example, in astronomy a telescope equipped with an AO system can compensate for atmospheric disturbances and wind shake of the telescope structure resulting in higher image resolution [1]–[4]. In microscopy, AO allows to correct for aberrations such as local variations of the refractive index of observed specimen. Especially confocal and multi-photon microscopes particularly benefit from the improved resolution for visualization of cellular structures and subcellular processes [5], [6]. In addition, recent results of AO for detection of eye diseases and in vitro retinal imaging on the cellular level show promising examination and treatment opportunities [7]–[9].

In general, an AO control loop consists of a wavefront sensor, a deformable mirror, and a wavefront reconstructor (see Fig. 1). In order to correct for optical aberrations, the wavefront sensor measures the optical phase deviations of the incoming wavefront. Afterwards, the wavefront reconstructor computes suitable DM deformations such that the optical aberrations are compensated when the light is being reflected from the deformed DM. Finally, the DM receives the deformation commands and needs to be deformed as fast as possible to achieve the desired optical correction. Depending on the field of application, the wavefront reconstructor can also be used to compute the phase profile of the incoming wavefront for visualization or analysis purposes. If the wavefront sensor measures the optical aberrations after the DM then a typical null-seeking AO control loop is achieved [2], [10]. The optical disturbance rejection bandwidth depends on the readout speed of the wavefront sensor, the computation speed of the wavefront reconstructor, and the bandwidth of the DM. In modern AO systems, e.g., Shack-Hartmann wavefront sensors with readout frequencies above 1 kHz are available. Also integrated circuits with specialized algorithms for wavefront reconstruction operate above 1 kHz [11]. Only the deformable membrane mirrors often show a bandwidth below 1 kHz and limit the achievable closed loop AO bandwidth.[1]

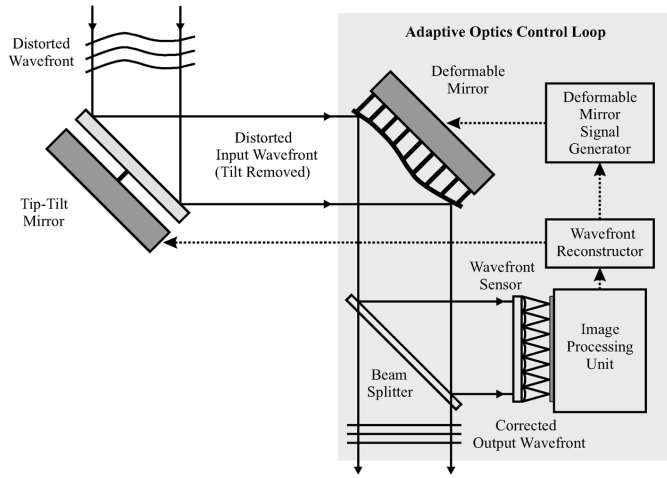

Fig. 1. Typical layout of an adaptive optics control loop with a deformable mirror, a wavefront sensor, and a wavefront reconstructor.

Today, membrane DMs usually consist of a thin reflective circular or rectangular membrane and underlying force actuators [12]–[15]. By applying a constant external voltage to the mirror actuators, the membrane is deformed locally. The resulting deformation usually lies in the range of a few micrometers. Depending on the field of application, the correction of optical aberration in AO systems requires high spatial and temporal resolution of the deformable mirror. Thereby, the spatial resolution strongly depends on the number and the location of the actuators and the material properties of the deformable membrane.

Manuscript received February 22, 2011; revised October 18, 2011 and January 19, 2012; accepted January 28, 2012. Manuscript received in final form January 30, 2012. Date of publication March 05, 2012; date of current version nulldate. Recommended by Associate Editor M. Fujita. This work was supported by the DFG under Grant SA-847/10-1 and Grant OS-111/29-1.

T. Ruppel and O. Sawodny are with the Institute for System Dynamics, University of Stuttgart, Stuttgart 70569, Germany (e-mail: thomas.ruppel@isys.uni-stuttgart.de).

S. Dong and W. Osten are with the Institut für Technische Optik, University of Stuttgart, Stuttgart 70569, Germany.

F. Rooms is with ALPAO, 38 330 Biviers, France.

Color versions of one or more of the figures in this paper are available online at http://ieeexplore.ieee.org.

Digital Object Identifier 10.1109/TCST.2012.2186813

[1]Pure feedback control of the mirror vibrations with a wavefront sensor measuring the actuator positions does not lead to satisfying results if the first resonances of the DM are close to the bandwidth of the AO loop.

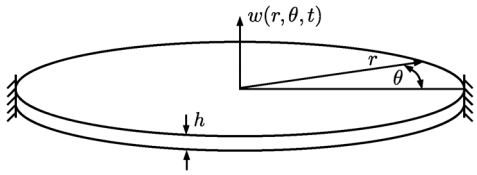

Fig. 2. Principle layout of the deformable mirror membrane with clamped outer edge.

The temporal resolution of the DM is mainly dominated by the boundary conditions of the membrane, its material properties, and the chosen actuators [16]. In case of non-contact actuators (e.g., electro-static, voice coils), the first resonances of the deformable membrane strongly limit the achievable temporal performance of the DM. In this case, feedforward control can be used to increase the bandwidth of the DM and make it applicable for high-level AO control systems.

The principle of model-based feedforward control for deformable mirrors was previously investigated in [17] and [18]. Thereby, performance enhancements in terms of reduced settling time and less overshoot are demonstrated for a 45 actuator prototype DM with internal position control. The dynamical model of the DM was identified based on internal position measurements of excited DM actuators. Unfortunately, this identification method cannot be applied to small scale membrane DMs. These elements do not include internal position sensors and complicate the model identification procedure. However, in this paper a practical identification procedure for membrane DMs with static interferometric measurements and dynamic measurements from a laser vibrometer are presented. It is shown that together with an identified dynamical model feedforward control can be employed for membrane DMs, also.

The structure of this paper is as follows. In Section II, a partial differential equation describing the membrane dynamics is presented. Based on an infinite dimensional series approximation of its homogeneous solution, the modal dynamics and analytical eigenfrequencies of the membrane are derived. In Section III, static measurements of the actuator influence functions are used to approximate the dynamic eigenmodes of the deformable membrane via principle component analysis (PCA). The PCA basis is used for damping identification in Section IV. Finally, feedforward control signals are computed in Section V and experimental results of feedforward control of a 88 actuator ALPAO DM are presented in Section VI.

II. Modeling of Deformable Mirrors

The deformable mirror investigated here (ALPAO DM88) is modeled as a circular plate of thickness h with finite radius a centered at the origin of the $r-\theta$ plane (Fig. 2). Hereby, r, θ are polar coordinates. The mirror is modeled as a plate in order to include a considerable out-of-plane stiffness in the model [19]. For dynamic analysis, a large deflection of the plate is not considered here and nonlinear effects such as tensile stresses of the plate are neglected [20], [21]. In the following, the time varying deflection of the plate is measured by $w(r,\theta,t)$ relative to the undeflected reference. The argument $t \in \mathbb{R}^+$ is the time. The governing equation for the mirror deformations can be mathematically described by a biharmonic partial differential equation (PDE) over the domain S: $r \in (0, a]$, $\theta \in (-\pi, +\pi]$ of the form

$$\left(D\nabla^4 + \mu\frac{\partial}{\partial t}\nabla^4 + \rho h\frac{\partial^2}{\partial t^2}\right) w(r,\theta,t) = u(r,\theta,t) \qquad (1)$$

with the operator $\nabla^4 = \nabla^2\nabla^2$, and ∇^2 being the Laplacian in polar coordinates

$$\nabla^4 = \left(\frac{\partial^2}{\partial r^2} + \frac{1}{r}\frac{\partial}{\partial r} + \frac{1}{r^2}\frac{\partial^2}{\partial\theta^2}\right)^2, \quad D = \frac{Eh^3}{12(1-\nu^2)}$$

where ρ is the material density, μ is the Kelvin-Voigt damping parameter, and E and ν are Young's modulus and Poisson's ratio, respectively. In (1) the external pressure is described by $u(r,\theta,t)$. By neglecting gravitational forces for point actuated deformable membranes, the external pressure u has the form

$$u(r,\theta,t) = \sum_{m=1}^{M} \frac{\hat{u}_m(t)}{r_m}\delta(r-r_m)\delta(\theta-\theta_m) \qquad (2)$$

with $\{r_i, \theta_i\}$ describing the actuator positions in polar coordinates and M being the number of actuators. The time-dependent actuator force is described by $\hat{u}_i(t)$ and δ is the Dirac delta function.[2] As verified by experiments, the relationship between the voice-coil actuator force and the voice-coil current can be assumed to be linear for the DM88 and high frequency dynamics of the voice-coils as well as delays due to digital analog conversion in the drive electronics of the DM can be neglected.

The boundary conditions of the plate at the outer edge $r = a$ read

$$w(a,\theta,t) = 0 \qquad (3a)$$

$$\frac{\partial}{\partial r}w(r,\theta,t)\bigg|_{r=a} = 0 \qquad (3b)$$

and correspond to a membrane clamped at the outer edge.

A. Modal Analysis

The homogeneous solution of the undamped PDE (1) with $u = 0$ and $\mu = 0$ can be parametrized by separation of variables as $w(r,\theta,t) = W(r,\theta)e^{(i\omega t)}$.[3] Thereby, the PDE (1) reduces to

$$\nabla^4 W(r,\theta) - \beta^4 W(r,\theta) = 0, \quad \beta^2 = \omega\sqrt{\frac{\rho h}{D}}. \qquad (4)$$

Equation (4) can be written in operator form

$$(\nabla^4 - \beta^4)W(r,\theta) = (\nabla^2 + \beta^2)(\nabla^2 - \beta^2)W(r,\theta) = 0 \qquad (5)$$

which leads to

$$(\nabla^2 - \beta^2)W(r,\theta) = W_1(r,\theta), \quad (\nabla^2 + \beta^2)W_1(r,\theta) = 0. \qquad (6)$$

[2]The normalization factor r_m corresponds to the Jacobian in cylinder coordinates fulfilling the integral property of the Dirac delta function.

[3]The modal solution of the undamped case can be used for the damped case since the biharmonic operator with clamped edge boundary conditions is self-adjoint and Kelvin-Voigt damping is a linear combination of the stiffness distribution (biharmonic operator) and the mass distribution (unity) in (1) [22].

Because β^2 is constant, the solution of the first equation of (6) is

$$W(r,\theta) = W_1(r,\theta) + W_2(r,\theta) \tag{7}$$

where $W_2(r,\theta)$ is the solution of the homogeneous equation

$$(\nabla^2 - \beta^2)W_2(r,\theta) = \left[\nabla^2 + (i\beta)^2\right] W_2(r,\theta) = 0. \tag{8}$$

The solutions of (6) and (8) are given in [22] by

$$\begin{aligned} W_{1,k}(r,\theta) &= [A_{1,k}J_k(\beta r) + A_{3,k}Y_k(\beta r)]\sin(k\theta) \\ &\quad + [A_{2,k}J_k(\beta r) + A_{4,k}Y_k(\beta r)]\cos(k\theta) \qquad (9a) \\ W_{2,k}(r,\theta) &= [B_{1,k}I_k(\beta r) + B_{3,k}K_k(\beta r)]\sin(k\theta) \\ &\quad + [B_{2,k}I_k(\beta r) + B_{4,k}K_k(\beta r)]\cos(k\theta) \qquad (9b) \end{aligned}$$

where $J_k(.)$ and $Y_k(.)$ are Bessel functions of order $k \in \mathbb{N}$ and of the first and second kind, respectively. For the second component $W_2(r,\theta)$, the functions $I_k(.)$ and $K_k(.)$ are modified or hyperbolic Bessel functions of order k and of the first and second kind, respectively. In order to fulfill the boundary conditions (3), the coefficients $A_{i,k}$ and $B_{i,k}$ $(i = 1,\ldots,4)$ must be determined appropriately.

For the case of a deformable membrane mirror with clamped edge at the outer radius a, the general solution (9) reduces to

$$\begin{aligned} W_k(r,\theta) &= [A_{1,k}J_k(\beta r) + B_{1,k}I_k(\beta r)]\sin(k\theta) \\ &\quad + [A_{2,k}J_k(\beta r) + B_{2,k}I_k(\beta r)]\cos(k\theta) \end{aligned} \tag{10}$$

because Bessel functions of the second kind, $Y_k(.)$ and $K_k(.)$ become infinite at $r = 0$. Using the boundary condition (3a) yields

$$B_{1,k} = -\frac{J_k(\beta a)}{I_k(\beta a)}A_{1,k}, \quad B_{2,k} = -\frac{J_k(\beta a)}{I_k(\beta a)}A_{2,k} \tag{11}$$

and

$$\begin{aligned} W_k(r,\theta) &= \left[J_k(\beta r) - \frac{J_k(\beta a)}{I_k(\beta a)}I_k(\beta r)\right] \\ &\quad \times \left(A_{1,k}\sin(k\theta) + A_{2,k}\cos(k\theta)\right). \end{aligned} \tag{12}$$

The boundary condition (3b) leads to the set of characteristic equations

$$\left[\frac{d}{dr}J_k(\beta r) - \frac{J_k(\beta a)}{I_k(\beta a)}\frac{d}{dr}I_k(\beta r)\right]\Bigg|_{r=a} = 0 \tag{13}$$

that can be simplified to the transcendent conditions

$$I_k(\beta a)J_{k-1}(\beta a) - J_k(\beta a)I_{k-1}(\beta a) = 0. \tag{14}$$

There are multiple solutions of (14) which have to be computed numerically. For each Bessel function order k there exist infinitely many $\beta_{k,n}$, $n \in \mathbb{N}$ that lead to the characteristic eigenfrequencies

$$\omega_{k,n} = \beta_{k,n}^2\sqrt{\frac{D}{\rho h}}. \tag{15}$$

For each eigenfrequency $\omega_{k,n}$ there are two orthogonal modes [sin(.) and cos(.)], except for $k = 0$, for which only one mode [cos(.)] is obtained (Fig. 3).

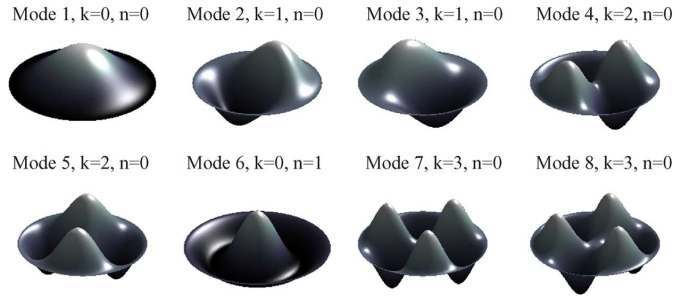

Fig. 3. Non-proportional visualization of the first eight analytical mirror eigenmodes ordered by increasing eigenvalue $\beta_{k,n}$, where k and n correspond to the circular and radial frequency, respectively.

The eigenfunctions are orthogonal (10) and can be normalized over the membrane domain S fulfilling

$$\iint_S W_i W_j \mathrm{d}S = \delta_{i,j} \tag{16}$$

$$\iint_S W_i \nabla^4 W_j \mathrm{d}S = \beta^4 \delta_{i,j} \tag{17}$$

where $\delta_{i,j}$ is the Kronecker delta. For a detailed study of the mathematical properties of the deformable mirror eigenmodes the reader is referred to [16], [19], and [23].

B. Series Approximation of the Infinite Dimensional Dynamics

In order to approximate the infinite dimensional system dynamics, a Fourier-Bessel expansion of the membrane displacement is used (1). In particular, the membrane displacement is approximated by

$$w^N(r,\theta,t) = \sum_{j=1}^{N} q_j(t)W_j(r,\theta) \tag{18}$$

where $W_j(r,\theta)$ are the orthonormal eigenfunctions ordered with increasing eigenvalue and $q_j(t)$ is the corresponding temporal modal amplitude.[4] The approximation number N is considered to be a finite number suitably large for accurately modeling the system dynamics. Since the spatial eigenfrequencies of the computed eigenfunctions increase both in radial and circular direction with increasing temporal eigenfrequency, proper sampling of available actuator positions give a reasonable number N in practice. Also, an upper bound for N can be found in practice by analyzing the static deformations of the deformable mirror when individual actuators are excited. The higher the number N is chosen, the smaller is the modal approximation error of the residual deformable mirror surface.

Introducing (18) in PDE (1) and recalling that the operator ∇^4 is linear one obtains

$$\begin{aligned} &\sum_{j=1}^{N} Dq_j(t)\nabla^4 W_j(r,\theta) + \sum_{j=1}^{N} \dot{q}_j(t)\mu\nabla^4 W_j(r,\theta) \\ &\qquad + \sum_{j=1}^{N} \rho h\ddot{q}_j(t)W_j(r,\theta) = u(r,\theta,t). \end{aligned} \tag{19}$$

[4]Due to the rearrangement of the computed modes, the modal index j is chosen to start at $j = 1$ instead of $j = 0$ in the following sections.

Multiplying both sides by the orthonormal eigenfunctions $W_k(r,\theta)$, $k = 1,\ldots,N$ and integrating over the membrane domain S reads

$$\begin{aligned}&\iint_S W_k(r,\theta)\sum_{j=1}^{N} Dq_j(t)\nabla^4 W_j(r,\theta)\mathrm{d}S\\ &+\iint_S W_k(r,\theta)\sum_{j=1}^{N}\mu\dot{q}_j(t)\nabla^4 W_j(r,\theta)\mathrm{d}S\\ &+\iint_S W_k(r,\theta)\sum_{j=1}^{N}\rho h\ddot{q}_j(t)W_j(r,\theta)\mathrm{d}S\\ &=\iint_S W_k(r,\theta)u(r,\theta,t)\mathrm{d}S.\end{aligned}\tag{20}$$

By changing order of integration and summation in (20) and using relations (16) and (17) the modal dynamics can be obtained as

$$\rho h\ddot{q}_k(t)+\mu_k\beta_k^2\dot{q}_k(t)+D\beta_k^4 q_k(t)=v_k(t),\quad k=1,\ldots,N\tag{21}$$

where $\mu_k = \mu\beta_k^2$ and $v_k(t)$ is the new modal input. Equation (21) represents a finite set of decoupled ordinary differential equations approximating the plate dynamics in modal coordinates. Recalling relation (2), the modal input $v_k(t)$ reads

$$v_k(t)=\iint_S W_k(r,\theta)\sum_{m=1}^{M}\frac{\hat{u}_m(t)}{r_m}\delta(r-r_m)\delta(\theta-\theta_m)\mathrm{d}S.\tag{22}$$

Finally, by using the shifting property of the delta function in the integral over domain S, (22) simplifies to

$$v_k(t)=\sum_{m=1}^{M}\hat{u}_m(t)W_k(r_m,\theta_m)\tag{23}$$

which corresponds to the sum of modal contributions of all M actuators to mode k. With (21) and (23) it can be seen that a suitable excitation of distributed actuators can be used to excite particular eigenmodes of the deformable mirror. This property is used to implement a modal feedforward controller independently driving the individual modes with suitable input commands. However, in order to compute the physical input commands for the DM88 both the real modal shapes of the mirror membrane and the modal contributions of each actuator must be determined. Therefore, in the next section the modal contributions are derived based on actuator influence function measurements and analysis.

III. Actuator Influence Function Measurements

A. Measurement Setup

Although the theoretic analysis of the membrane dynamics in Section II-A and the modal contributions of each actuator (23) would allow to develop a feedforward controller already, in particular the damping parameter μ_k needs to be determined for the considered modes in practice. For modal damping identification, a particular mode is excited by combining all physical inputs [see (23)] appropriately and the damping parameter is estimated based on the measured modal response.

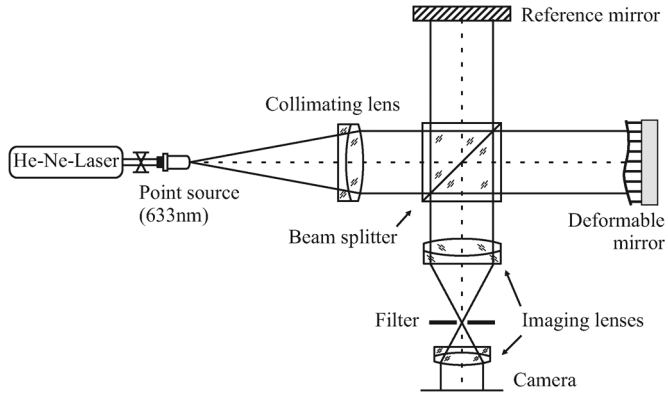

Fig. 4. Actuator influence function measurement setup with a Twyman-Green interferometer and the ALPAO DM88 deformable mirror.

In order to obtain suitable input commands for the excitation of specific eigenmodes, the modal contributions in (23) are derived via static actuator influence function measurements and analysis. The measurements are performed with a standard phase-shifting interferometer. The interferometer is constructed in Twyman-Green geometry ($\lambda = 633$ nm, 2048×2048 pixel CCD camera), and a $4-f$ relay system is employed to image the DM surface as shown in Fig. 4. Thereby, the mirror deflection $w(r,\theta,t)$ is sampled over the domain S at specific measurement points (r_i,θ_i). During the measurements, each actuator is triggered with a voltage of 0.25 V to obtain the deformation and a five step phase shifting method is then used to get the corresponding height map. For eliminating the aberration introduced by the interferometer and the undeflected mirror, the height map of a reference surface where no voltage is applied to the actuators is subtracted to obtain the final influence function. With this technique, the surface of the DM can be measured within a range of several hundred micrometers and a resolution of 100 nm peak-to-valley. Although for some AO systems the DM surface must be known within a few nanometers, a resolution of 100 nm is sufficient here since the DM88 is specified to operate within tens of micrometers surface deflection. For the following computations, the high resolution images are scaled down to 305×305 pixels per image allowing memory-demanding operations as e.g. singular value decompositions of multiple images on a modern desktop PC. Thereby, the surface deflection is described by y_i, $i = 1,\ldots,93\,025$ measurement points.

The frame rate of the white light interferometer does not allow to measure the transient behavior of the membrane. Therefore, only the static displacement of individually excited actuators can be measured leading to the output equation with discretized surface deflection points y_i over the CCD camera

$$y_i=\iint_S w(r,\theta)\frac{1}{r_i}\delta(r-r_i)\delta(\theta-\theta_i)\mathrm{d}S.\tag{24}$$

Using the series approximation (18), (24) can be simplified to

$$y_i=\sum_{j=1}^{N} q_j W_j(r_i,\theta_i).\tag{25}$$

Now, taking into account the relationship between physical inputs and modal amplitudes (21) and (23) for the static case $\ddot{q} = 0$ and $\dot{q} = 0$ one obtains

$$q_j = \frac{1}{D\beta_j^4} \sum_{m=1}^{M} \hat{u}_m W_j(r_m, \theta_m). \tag{26}$$

By inserting (26) in (24), the static input output relation between actuator excitation $\hat{u}_m$ and surface measurement y_i can be derived as

$$y_i = \sum_{j=1}^{N} \left(\frac{1}{D\beta_j^4} \sum_{m=1}^{M} \hat{u}_m W_j(r_m, \theta_m) \right) W_j(r_i, \theta_i). \tag{27}$$

Now, the finite dimensional input output relation (27) is used to apply a principle component analysis on the actuator influence functions in order to compute the modal contributions $\hat{u}_m$ in relation to the infinite dimensional PDE model.

Writing the double sum in (27) in a matrix vector notation yields

$$y_i = \Psi_{N,i} \Delta \Omega_N^T \hat{u} \tag{28}$$

where

$$\Psi_{N,i} = \begin{bmatrix} W_1(r_i, \theta_i) & \dots & W_N(r_i, \theta_i) \end{bmatrix}$$

$$\Delta = \begin{bmatrix} \frac{1}{D\beta_1^4} & & \\ & \ddots & \\ & & \frac{1}{D\beta_N^4} \end{bmatrix}$$

$$\Omega_N^T = \begin{bmatrix} W_1(r_1, \theta_1) & \dots & W_1(r_M, \theta_M) \\ \vdots & \ddots & \vdots \\ W_N(r_1, \theta_1) & \dots & W_N(r_M, \theta_M) \end{bmatrix}$$

$$\hat{u} = \begin{bmatrix} \hat{u}_1 & \dots & \hat{u}_M \end{bmatrix}^T.$$

Combining all measurement points of a single measurement with a specific input command $\hat{u}^T$ in the measurement vector $y \in \mathbb{R}^{N_y}$, $N_y = 93\,025$ leads to

$$y = \begin{bmatrix} y_1 \\ \vdots \\ y_{N_y} \end{bmatrix} = \Psi_N \Delta \Omega_N^T \hat{u} \tag{29}$$

where

$$\Psi_N = \begin{bmatrix} W_1(r_1, \theta_1) & \dots & W_N(r_1, \theta_1) \\ \vdots & \ddots & \vdots \\ W_1\left(r_{N_y}, \theta_{N_y}\right) & \dots & W_N\left(r_{N_y}, \theta_{N_y}\right) \end{bmatrix}.$$

Exemplary measurements of actuator influence functions (columns of Ψ_N) are shown in Fig. 5. Due to the clamped edge boundary condition of the DM membrane, actuators located at the edge of the DM cause a smaller deflection of the membrane than actuators at the center using similar forces. For comparison, the geometric layout of the DM88 actuator pattern is shown in Fig. 6.

When combining all measurements y in a single measurement matrix Y and choosing the excitation signals as shown in the input matrix $\hat{U}$ one obtains

$$Y = \Psi_N \Delta \Omega_N^T \underbrace{\begin{bmatrix} 1 & 0 & 0 \\ \vdots & \ddots & \vdots \\ 0 & 0 & 1 \end{bmatrix}}_{\hat{U}} = \Psi_N \Delta \Omega_N^T \tag{30}$$

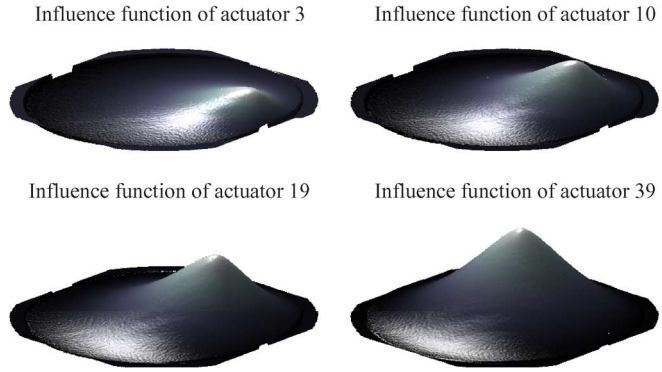

Fig. 5. Non-proportional visualization of selected ALPAO DM88 actuator influence functions measured via white light interferometry.

where Y is a $[N_y \times M]$ matrix with condition number 196 containing all actuator influence function measurements and $\hat{U}$ is a $[M \times M]$ unity matrix containing all normalized excitation signals. The measurement equation (30) contains both a projection matrix Ω_N^T from actuator commands to eigenmodes and a projection matrix Ψ_N from eigenmodes to measurement points. In the following section, a principle component analysis of the measurement matrix Y will be performed to approximate the shape of the first $M = 88$ eigenmodes $W_j(r, \theta)$ and the entries of the corresponding projection matrix Ω_N^T.

B. Principle Component Analysis of Actuator Influence Functions

The matrix of actuator influence functions Y spans the controllable subspace of static mirror deformations that can be excited by the available 88 actuators of the DM88. Finding a linear combination of these actuator influence functions such that the dynamic eigenmodes of the DM88 can be excited individually is accomplished in terms of an eigenvector-based multivariate analysis of Y. By performing a principle component analysis (PCA) of the measurement matrix Y, the correlated influence function measurements are converted into a set of uncorrelated variables called principle components [24]. The PCA of Y can be related to the singular value decomposition of Y with

$$\text{svd}\{Y\} = W \Sigma V^T \tag{31}$$

where W is a $[N_y \times N_y]$ matrix of eigenvectors of YY^T, Σ is a $[N_y \times M]$ matrix with nonnegative real numbers (singular values) on its diagonal, and V is a $[M \times M]$ matrix which is in close relation to (30).[5] However, (30) and (31) are not completely similar because the subspaces spanned by Ψ_N and Ω_N^T are not orthogonal over the finite grid of the $M = 88$ actuator influence function measurements. Therefore, the PCA will only give approximate values of the entries of Ω_N^T.

With (31), the PCA transformation of Y preserving dimensionality is given by

$$X^T = Y^T W \tag{32}$$

[5]In fact, it can be shown that the left singular vectors of Y correspond to the right singular vectors of the stiffness matrix of the lumped parameter system approximation of PDE (1).

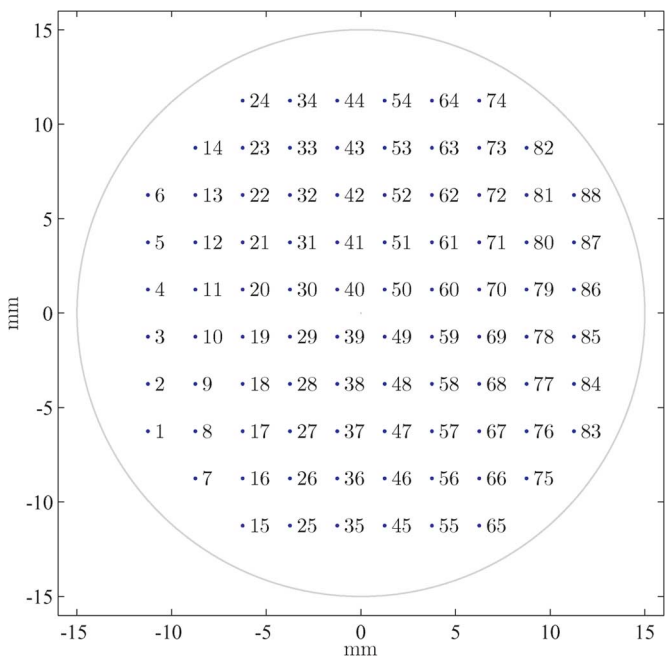

Fig. 6. Geometric layout and numbering of the ALPAO DM88 voice coil actuator positions.

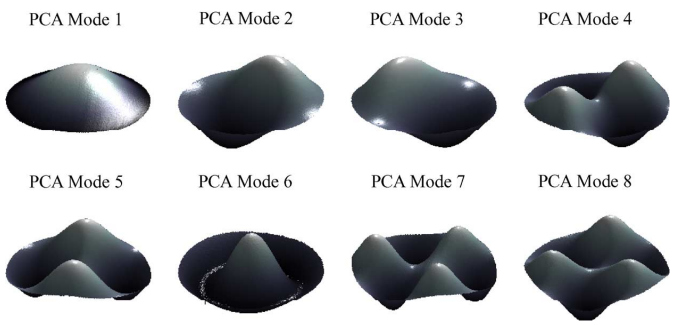

Fig. 7. Non-proportional visualization of the first eight static PCA modes ordered by increasing eigenvalue.

where X is a matrix consisting of 88 vectors being the projection of the corresponding data vector from matrix Y onto the basis vectors contained in the columns of matrix W. The rows of X contain the scores of the measurements with respect to the principle components in W and correspond to actuator commands resulting in a deformation described in W. In practice, it can be found that the left singular vectors W resemble the sampled dynamic eigenmodes (9) very well. Subsequently, Ω_N^T can be approximated by optically measured actuator influence functions and X contains the necessary information for exciting specific eigenmodes for damping identification. The left singular vectors W derived in (31) are visualized in Fig. 7 ordered by increasing singular values. Clearly, the PCA basis shows similar features as the dynamic eigenmodes in Fig. 3. Due to this direct relation, the PCA basis (also containing the appropriate actuator commands in X) is used for dynamic identification of modal damping in the following section.

IV. Damping Identification

Recalling the decoupled modal dynamics (21) of the DM, the eigenfrequency and damping parameters of the individual eigenmodes can be matched to models of the form

$$\ddot{q}_j(t) + \mu_j^* \omega_j \dot{q}_j(t) + \omega_j^2 q_j(t) = b^* v_j(t) \tag{33}$$

where ω_j is the modal eigenfrequency of mode j, $\mu_j^* = \mu_j/D$, and $b^* = 1/(\rho h)$ [25].

The structural damping of the ALPAO DM88 mirror eigenmodes are identified via step response measurements of the mirror surface deflection. In particular, the actuator commands are created based on the spatial PCA basis multiplied by a temporal step function. The time-varying surface deflection is measured point-wise with a laser-vibrometer at a sampling frequency of 100 kHz. The optimal measurement position for damping identification is at the maximum deflection of the PCA mode. For the first PCA mode, the measurement point is in the center of the DM. For the second PCA mode, the measurement point is approximately at half the radius of the DM. Special attention must be drawn to the angular position of the measurement point for the second PCA mode since the PCA mode exhibits two angular nodes of zero deflection at $\theta = 0$ and $\theta = \pi$. The measurement results of the surface velocity, the integrated position signal, and a frequency analysis of the step response of the first and second PCA mode at representative positions are illustrated in Figs. 8 and 9.

In Fig. 8, the dominant resonance of the first PCA mode can be found at 290.5 Hz. A second resonance at 1040 Hz is also excited by the PCA basis showing the spillover effect of the 88 concentrated inputs. In Fig. 9, spillover characteristics are not visible for the second PCA mode. In particular, the second PCA mode excites a resonance frequency at 584.4 Hz. For both PCA modes, the damping coefficients are determined by minimizing the L_2 norm between modal measurement and modal simulation of the step response. The corresponding coefficients are listed in Table II.

In comparison to the analytical eigenfrequencies in Table I, the measured eigenfrequencies are approximately 50 Hz higher than expected. This characteristic is mainly due to an unmodeled initial tension of the deformable membrane that is a side-effect of the manufacturing process. Also, the unexpectedly high damping of the first PCA mode may be due to an initial tension of the deformable membrane.

V. Feedforward Signal Generation

By having suitable modal models for the dynamic behavior of the mirror, it is possible to design a feedforward controller for set-point changes of the membrane DM in modal coordinates. According to (27), is assumed that the initial and the desired mirror deformations can be expressed in vectors of sampled surface displacements y_0 and y_f, respectively. The vectors of initial and final modal coordinates q_0 and q_f can be computed with (32) as

$$q_0 = W^T y_0, \quad q_f = W^T y_f. \tag{34}$$

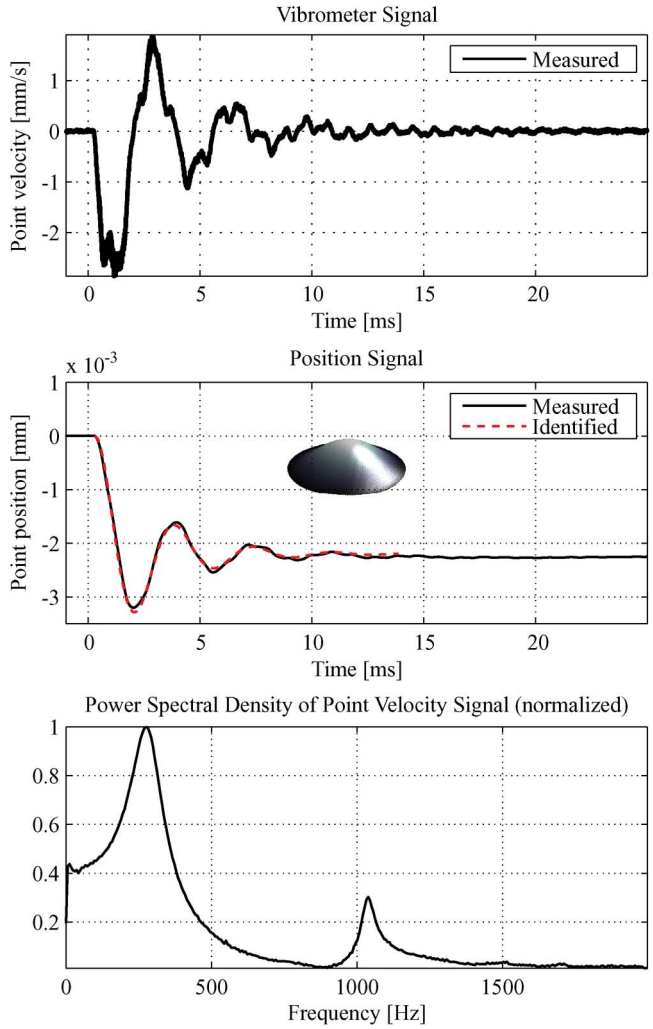

Fig. 8. Point-wise step response measurement and frequency analysis of the first PCA mode of the ALPAO DM88.

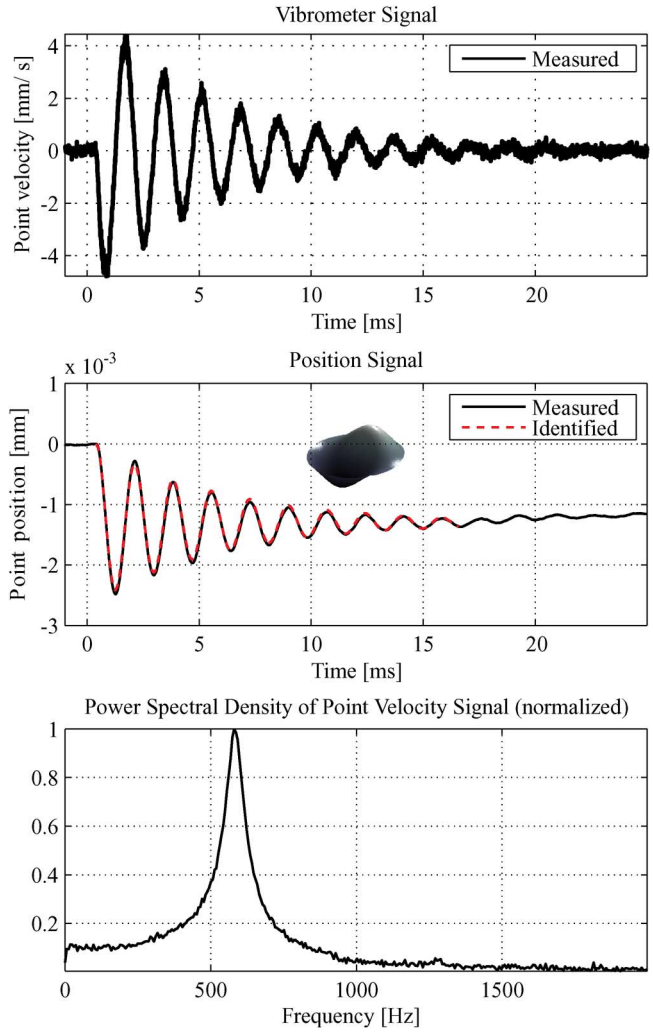

Fig. 9. Point-wise step response measurement and frequency analysis of the second PCA mode of the ALPAO DM88.

In [17], modal trajectory generation for set-point changes of large deformable mirrors with modal dynamics modeled as linear time invariant second order systems with maximal relative degree is introduced. Thereby, the main idea is to drive the DM from one static deformation to another one by accounting for its transient behavior in the input signal rather than by local error feedback. Since the stiffness and damping parameters of membrane DMs can be determined as shown in Sections III and IV, the feedforward signal generation can be adopted here.

With the series approximation (18) and identified modal stiffness and damping parameters, (33) can be used to compute the modal inputs $v_j(t)$ as

$$v_j^d(t) = \frac{1}{b^*}\left(\ddot{q}_j^d(t) + \mu_j^* \omega_j \dot{q}_j^d(t) + \omega_j^2 q_j^d(t)\right) \tag{35}$$

where $q_j^d(t) \in \mathcal{C}^2$ is a sufficiently smooth output trajectory connecting $q_{0,j}$ and $q_{f,j}$ in modal coordinates. The desired modal outputs are generated as

$$q_j^d(t) = q_{0,j} + (q_{f,j} - q_{0,j})\kappa(t), \quad t \in [t_0, t_1] \tag{36}$$

with $\kappa(t)$ as shown in Fig. 10 and (37) at the bottom of the next page.

TABLE I
ANALYTICAL EIGENFREQUENCIES OF THE ALPAO DM88 FOR THE FIRST EIGHT EIGENMODES

Mode	Eigenfrequency (Hz)
1	252.1
2	524.5
3	524.5
4	860.5
5	860.5
6	981.2
7	1259.0
8	1259.0

TABLE II
IDENTIFIED EIGENFREQUENCY AND MODAL DAMPING PARAMETERS OF THE FIRST TWO EIGENMODES OF THE ALPAO DM88

	Eigenfrequency (Hz)	Damping parameter μ_j^*
Mode 1	290.6	0.42
Mode 2	584.4	0.096

Although a polynomial degree of $k = 3$ would be sufficient to generate $\mathcal{C}^2$ continuous modal output trajectories, the polynomial degree $k = 5$ is chosen to account for the inherent but

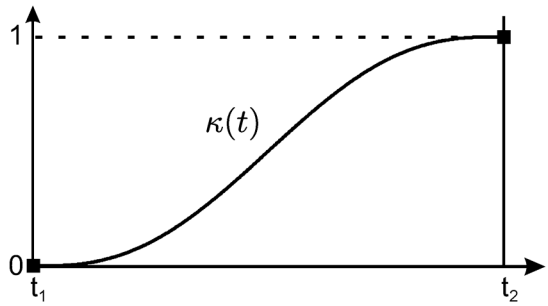

Fig. 10. Transition polynomial $\kappa(t), t \in [t_1, t_2]$ for a modal set-point change of the ALPAO DM88.

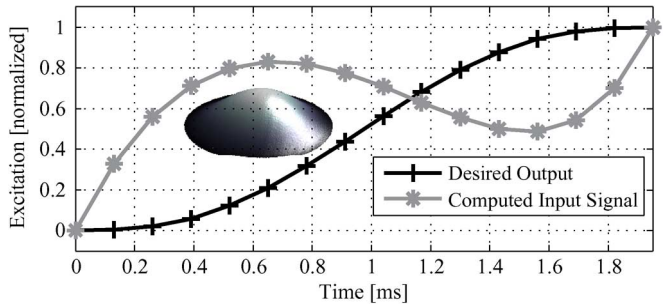

Fig. 11. Desired modal output and modal feedforward control command for a set-point change of the first PCA mode of the ALPAO DM88 with a transition time of 1.96 ms.

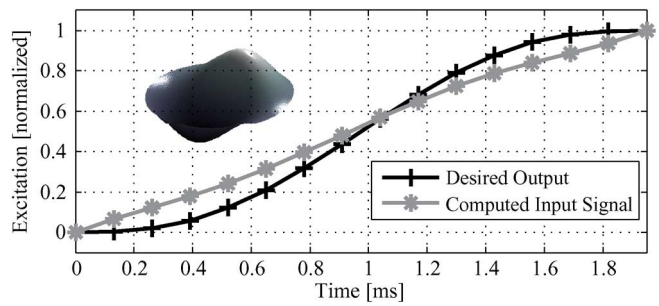

Fig. 12. Desired modal output and modal feedforward control command for a set-point change of the second PCA mode of the ALPAO DM88 with a transition time of 1.96 ms.

neglected dynamics of the voice-coil actuators of the ALPAO DM88.

The mapping from modal inputs v_j to actuator commands u_j can be performed with (23), where $W_j(r_j, \theta_j)$ is replaced by the approximation V^T of Ω_N^T from (31). In order to apply the time-varying input commands to the ALPAO DM88, an internal command buffer of a PC-based digital IO card connected to the DM electronics is used. The buffer can store up to 1024 values per actuator with a sampling rate of 0.13 ms. With (35)–(37), the feedforward commands can be computed offline and transferred to the DM with the digital IO card accessible from MATLAB.

In order to account for input constraints of the voice coil actuators, the transition time $t_2 - t_1$ of the feedforward control command must be chosen sufficiently large. If additional constraints are given for the time derivatives of the input signal, then time derivatives of (36) and (35) can be used to compute the maximum values of the feedforward commands. As visible in (37), a nth order time derivative of the transition polynomial scales with order n of the transition time. With (36) and (35), a parameter optimization of the transition can be implemented to find a time-optimal solution under input constraints of the feedforward control problem. However, for feedforward control of the ALPAO DM88 the transition time is chosen based on a sufficiently smooth temporal sampling of the input signal due to the buffer readout intervals of 0.13 ms. By experimental validation, the transition time is chosen to be 1.96 ms allowing for 15 sampling points within the feedforward command.

VI. Experimental Results

In order to show the efficiency of feedforward control for membrane DMs, a set-point change for the first two eigenmodes of the ALPAO DM88 is demonstrated. The eigenfrequencies of these two modes are at approximately 290 and 584 Hz.[6] The control objective is to apply a set-point change of 0.15 μm for mode 1 and 4 μm for mode 2 with a transition time of 1.96 ms. The amplitudes of the modal excitations were chosen such that the full measurement range of the vibrometer was exploited. Due to the internal buffer sampling time of 0.13 ms, the sampled feedforward control signals exhibit sufficiently smooth characteristics with 15 sampling points during this transition. For faster settling times, a higher temporal sampling would be necessary. The desired modal output trajectory and the computed modal input trajectories for the first and second PCA mode are illustrated in Figs. 11 and 12.

Similar to Section IV, the DM deflection is measured pointwise with a laser-vibrometer at a sampling frequency of 100 kHz. For the first PCA mode, the measurement point is located at the center of the DM. For the second PCA mode, a point located at the maximal deflection of the eigenmode is chosen close to half the radius of the DM. As visible in Figs. 8 and 9,

[6]When using only the first eigenmodes for feedforward control of arbitrary mirror deformations in practice, the dynamics of higher order modes are assumed to be quasi-stationary.

$$\kappa(t) = \begin{cases} 0, & \text{if } \leq (t_1 - t_0) \\ \frac{(2k+1)!}{k!(t_1-t_0)^{2k+1}} \sum_{i=0}^{k} \frac{(-1)^{k-i}}{i!(k-i)!(2k-i+1)} (t_1 - t_0)^i t^{2k-i+1}, & \text{if } 0 \leq t \leq (t_1 - t_0) \\ 1, & \text{if } t \geq (t_1 - t_0). \end{cases} \tag{37}$$

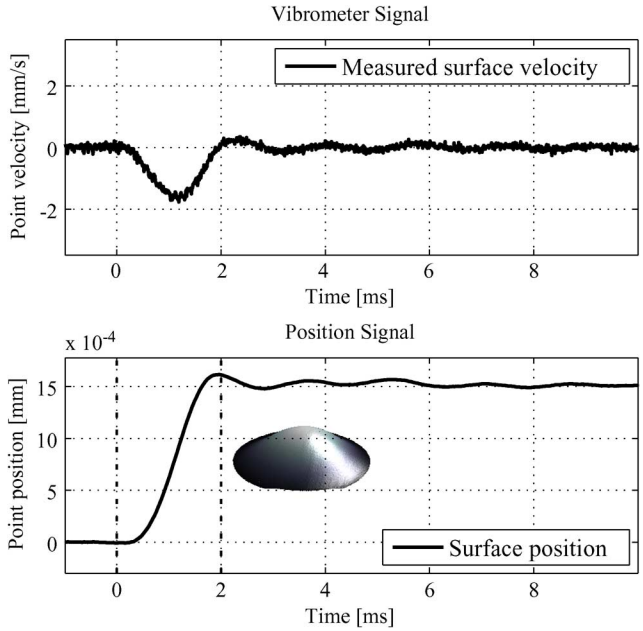

Fig. 13. Point-wise measurement results with feedforward control of the first PCA mode of the ALPAO DM88.

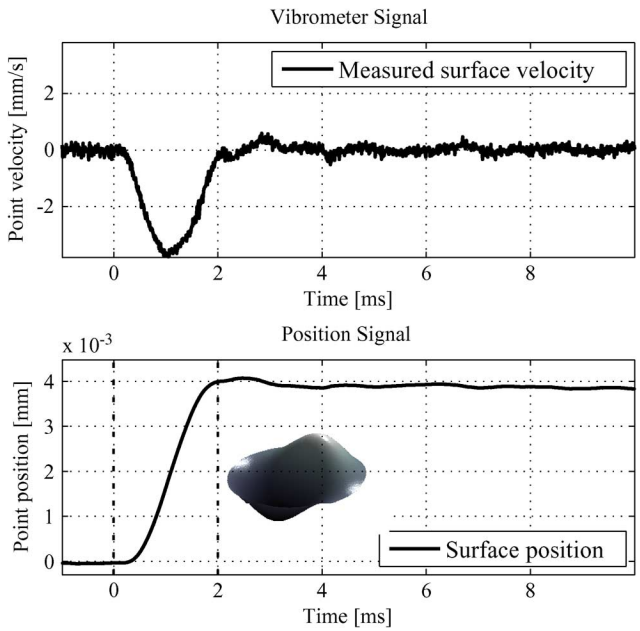

Fig. 14. Point-wise measurement results with feedforward control of the second PCA mode of the ALPAO DM88.

the typical settling time of the first two resonant modes without feedforward control is in the range of 10 ms. The measurement results with feedforward control are shown in Figs. 13 and 14.

In general, the number of modes considered for feedforward control depends on the desired settling time and the structural damping of the deformable mirror. All resonant modes showing a settling time above the desired transition time for set-point changes can be controlled via feedforward control. The computational effort scales linearly with the number of modes considered and can be implemented in parallel processes if needed. Thereby, the surface deformation can be mapped to PCA eigenmodes with (32) derived from static actuator influence function measurements. For the DM88, the first two resonant modes exhibit a settling time above 2 ms and were therefore considered for feedforward control. In experimental results, higher order modes proved to be well-damped and are therefore neglected in this study.

In comparison to the DM response without feedforward control it can clearly be seen that both the settling time and the overshoot of the DM88 are reduced effectively. However, it can also be seen that the static approximation of the dynamic DM eigenmodes via PCA modes partly leads to modal crosstalk and high frequency oscillations of the DM when the feedforward control signal is applied.

Concerning the robustness of the proposed approach, it must be noted that it is a pure feedforward control scheme without any feedback. Therefore, uncertain plant dynamics lead to less effective tracking performance but can not lead to instability of the system. If feedback can be implemented, the interested reader is referred to [26] and [27] for a detailed analysis of robust tracking performance with feedforward control under model uncertainties.

VII. Conclusion

In this paper, a detailed dynamical model for a deformable membrane mirror with concentrated inputs is presented. Based on a finite dimensional series approximation of the resulting PDE, the dominant modal dynamics of the deformable membrane are deduced. It is shown that the modal dynamics of the DM can be approximated by second-order ordinary differential equations with modal inputs. Using an eigenvector-based multivariate analysis of the static actuator influence functions, the theoretical modal inputs can be deduced experimentally. After performing a modal parameter identification based on the determined modal inputs, it is shown that modal feedforward control can be used to improve the performance of membrane DMs effectively. Thereby, the computed modal input commands are transformed into physical actuator commands with an inverse modal transformation based on a principle component analysis of measured actuator influence functions.

By using feedforward control, the dominant dynamics of the DM can be controlled allowing for faster settling times and reduced membrane vibrations after set-point changes. Experimental results show that for an ALPAO DM with 88 distributed actuators on a circular membrane the settling time can be reduced from 10 to 2 ms. Thereby, the feedforward control scheme is applied to the first two resonant modes of the DM. If a sufficiently high temporal sampling of the time-varying feedforward command is possible then this method can also be used to control higher order eigenmodes. In general, the presented method can be used for a wide variety of deformable mirrors ranging from large scale deformable secondary mirrors in astronomical telescopes to small scale deformable mirrors employed for AO microscopy, opthalmology, or beam shaping applications.

The presented method is easy to implement and shows great potential for performance enhancements of future deformable mirrors. Although a detailed dynamic identification of the

deformable mirror is necessary, the identification can be performed with standard hardware and the feedforward control strategy can be implemented in the control electronics that are being used for driving deformable mirrors, already.

ACKNOWLEDGMENT

The authors would like to thank all reviewers for their valuable comments and support on improving the quality of this paper.

REFERENCES

[1] E. P. Wallner, "Optimal wave-front correction using slope measurements," *J. Opt. Soc. Amer.*, vol. 73, no. 12, pp. 1771–1776, 1983.
[2] R. Tyson, *Adaptive Optics Engineering Handbook*. Boca Raton, FL: CRC Press, 2000.
[3] B. Frazier and R. Tyson, "Robust control of an adaptive optics system," in *Proc. 34th Southeastern Symp. Syst. Theory*, 2002, pp. 293–296.
[4] H. M. Martin, G. Brusa Zappellini, B. Cuerden, S. M. Miller, A. Riccardi, and B. K. Smith, "Deformable secondary mirrors for the LBT adaptive optics system," in *Advances in Adaptive Optics II*, D. Ellerbroek, L. Brent, and B. Calia, Eds., July 2006, vol. 6272, Ser. Proc. SPIE, p. 0U.
[5] M. Booth, M. Neil, R. Juškaitis, and T. Wilson, "Adaptive aberration correction in a confocal microscope," in *Proc. Nat. Acad. Sci. USA*, 2002, p. 5788.
[6] M. Booth, "Adaptive optics in microscopy," *Philosophical Trans. Royal Soc. A: Math., Phys., Eng. Sci.*, vol. 365, no. 1861, p. 2829, 2007.
[7] J. Liang, D. R. Williams, and D. T. Miller, "Supernormal vision and high-resolution retinal imaging through adaptive optics," *J. Opt. Soc. Amer. A*, vol. 14, no. 11, pp. 2884–2892, Nov. 1997.
[8] A. Roorda, F. Romero-Borja, I. William Donnelly, H. Queener, T. Hebert, and M. Campbell, "Adaptive optics scanning laser ophthalmoscopy," *Opt. Expr.*, vol. 10, no. 9, pp. 405–412, May 2002.
[9] D. C. Gray, W. Merigan, J. I. Wolfing, B. P. Gee, J. Porter, A. Dubra, T. H. Twietmeyer, K. Ahamd, R. Tumbar, F. Reinholz, and D. R. Williams, "In vivo fluorescence imaging of primate retinal ganglion cells and retinal pigment epithelial cells," *Opt. Expr.*, vol. 14, no. 16, pp. 7144–7158, Aug. 2006.
[10] D. Looze, "Minimum variance control structure for adaptive optics systems," in *Proc. Amer. Control Conf.*, 2005, pp. 1466–1471.
[11] R. Biasi, M. Andrighettoni, D. Veronese, V. Biliotti, L. Fini, A. Riccardi, P. Mantegazza, and D. Gallieni, "Lbt adaptive secondary electronics," in *SPIE*, P. L. Wizinowich and D. Bonaccini, Eds., 2003, vol. 4839, no. 1, pp. 772–782.
[12] E. Fernandez and P. Artal, "Membrane deformable mirror for adaptive optics: Performance limits in visual optics," *Opt. Expr.*, vol. 11, no. 9, pp. 1056–1069, May 2003.
[13] K. Bush, D. German, B. Klemme, A. Marrs, and M. Schoen, "Electrostatic membrane deformable mirror wavefront control systems: Design and analysis," in *Society of Photo-Optical Instrumentation Engineers (SPIE) Conference Series*, J. D. Gonglewski, M. T. Gruneisen, and M. K. Giles, Eds., Oct. 2004, vol. 5553, Ser. Presented at the Society of Photo-Optical Instrumentation Engineers (SPIE) Conference, pp. 28–38.
[14] G. Vdovin, "Micromachined membrane deformable mirrors," in *Adaptive Optics for Industry and Medicine*, ser. Springer Proceedings in Physics, U. Wittrock, Ed. New York: Springer Berlin Heidelberg, 2005, vol. 102, pp. 3–8.
[15] G. Vdovin, O. Soloviev, A. Samokhin, and M. Loktev, "Correction of low order aberrations using continuous deformable mirrors," *Opt. Exp.*, vol. 16, no. 5, pp. 2859–2866, 2008.
[16] T. Ruppel, O. Sawodny, and W. Osten, "Actuator placement for minimum force modal control of continuous faceplate deformable mirrors," in *Proc. IEEE Int. Conf. Control Appl. (CCA)*, 2010, pp. 867–872.
[17] T. Ruppel, M. Lloyd-Hart, D. Zanotti, and O. Sawodny, "Modal trajectory generation for adaptive secondary mirrors in astronomical adaptive optics," in *Proc. IEEE Int. Conf. Autom. Sci. Eng. (CASE)*, 2007, pp. 430–435.
[18] T. Ruppel, W. Osten, and O. Sawodny, "Model-based feedforward control of large deformable mirrors," *Euro. J. Control*, vol. 17, no. 3, pp. 261–272, 2011.
[19] K. Graff, *Wave Motion in Elastic Solids*. New York: Dover, 1991.
[20] J. Juillard and E. Colinet, "Modelling of nonlinear circular plates using modal analysis: Simulation and model validation," *J. Micromechan. Microeng.*, vol. 16, no. 2, p. 448, 2006.
[21] E. Cerda and L. Mahadevan, "Geometry and physics of wrinkling," *Phys. Rev. Lett.*, vol. 90, no. 7, p. 074 302, Feb. 2003.
[22] L. Meirovitch, *Analytical Methods in Vibration*. New York: The McMillan Company, 1967.
[23] O. Farrell and B. Ross, *Solved Problems: Gamma and Beta Functions, Legendre Polynomials, Bessel Functions*. New York: Macmillan, 1963.
[24] I. Jolliffe, *Principal Component Analysis*. New York: Wiley, 2002.
[25] P. L. Gatti and V. Ferrari, *Applied Structural and Mechanical Vibrations*. London, U.K.: E & FN Spon Press, 1999.
[26] S. Devasia, "Should model-based inverse inputs be used as feedforward under plant uncertainty?," *IEEE Trans. Autom. Control*, vol. 47, no. 11, pp. 1865–1871, Nov. 2002.
[27] V. Hagenmeyer, "Robust nonlinear tracking control based on differential flatness," *at-Automatisierungstechnik*, vol. 50, no. 12/2002, p. 615, 2002.

Thomas Ruppel received the Dipl.Ing. degree in engineering cybernetics from the University of Stuttgart, Stuttgart, Germany, in 2007.

He worked on the multi-mirror-telescope deformable mirror control systems as a DAAD scholar at the Optical Science Center, Tucson, AZ, from 2006 to 2007. Since 2007, he has been holding a Ph.D. research position with the Institute for System Dynamics, University of Stuttgart. His main research interests include control of adaptive optics systems, control of distributed parameter systems, trajectory generation methods, and flatness-based control of linear and nonlinear systems.

Shihao Dong received the B.E. degree from Tianjin University, Tianjin, China, in 2006 and the M.E. degree from COE, Shenzhen University, Guangdong, China, in 2009.

Currently, he is part of the Active Optical Systems Group, Institut für Technische Optik, University of Stuttgart, Stuttgart, Germany. His research interests include adaptive optics, digital image processing, and optical measurement systems.

Frédéric Rooms received the diploma of engineering in telecommunications from the Université Libre of Brussels, Brussels, Belgium, in 2000. He started his Ph.D. thesis at the Institut National Polytechnique of Grenoble, Grenoble, Spain. The aim was to develop an optical beam combiner for applications in astrophysics.

He is with ALPAO, Biviers, France. ALPAO is a manufacturer of deformable mirrors and adaptive optics systems. In 2003, he joined a French startup where he developed novel optical components. Nowadays, his research interests include ALPAO are the development and the control of deformable mirrors.

Wolfgang Osten received the Ph.D. degree from the Martin-Luther-University Halle-Wittenberg, Germany, in 1983.

From 1979 to 1991, he was working in the field of experimental stress analysis and optical metrology at the Institute of Mechanics and the Central Institute of Cybernetics and Information Processes, Berlin, Germany. In 1991, he joined the Bremen Institute of Applied Beam Technology (BIAS). Since September 2002, he has been a Full Professor with the University of Stuttgart, Stuttgart, Germany, and Director of the Institut für Technische Optik. His research work is focused on new concepts for industrial inspection and metrology by combining modern principles of optical metrology, sensor technology, and image processing. Special attention is paid to the development of resolution enhanced technologies for the investigation of micro and nano structures.

Oliver Sawodny received the Dipl.Ing. degree in electrical engineering from the University of Karlsruhe, Karlsruhe, Germany, in 1991, and the Ph.D. degree from the University of Ulm, Ulm, Germany, in 1996.

In 2002, he became a Full Professor with the Technical University of Ilmenau, Ilmenau, Germany. Since 2005, he has been the Director of the Institute for System Dynamics, University of Stuttgart, Stuttgart, Germany. His current research interests include methods of differential geometry, trajectory generation, and applications to mechatronic systems.